Density functional calculation of activation energies for lattice and grain boundary diffusion in alumina

Yinkai Lei, Yu Gong, Zhiyao Duan, and Guofeng Wang*

Department of Mechanical Engineering and Materials Science, University of Pittsburgh, Pittsburgh, Pennsylvania 15261, USA

(Received 23 September 2012; revised manuscript received 1 February 2013; published 19 June 2013)

To acquire knowledge on the lattice and grain boundary diffusion processes in alumina, we have determined the activation energies of elementary O and Al diffusive jumps in the bulk crystal, $\Sigma3(0001)$ grain boundaries, and $\Sigma3(10\bar{1}0)$ grain boundaries of α-Al_2O_3 using the first-principles density functional theory method. Specifically, we calculated the activation energies for four elementary jumps of both O and Al lattice diffusion in alumina. It was predicted that the activation energy of O lattice diffusion varied from 3.58 to 5.03 eV, while the activation energy of Al lattice diffusion ranged from 1.80 to 3.17 eV. As compared with experimental measurements, the theoretical predictions of the activation energy for lattice diffusion were lower and thus implied that there might be other high-energy diffusive jumps in the experimental alumina samples. Moreover, our results suggested that the Al lattice diffusion was faster than the O lattice diffusion in alumina, in agreement with experiment observations. Furthermore, it was found from our calculations for α-Al_2O_3 that the activation energies of O and Al grain boundary diffusion in the high-energy $\Sigma3(0001)$ grain boundaries were significantly lower than those of the lattice diffusion. In contrast, the activation energies of O and Al grain boundary diffusion in the low-energy $\Sigma3(10\bar{1}0)$ grain boundaries could be even higher than those of the lattice diffusion.

DOI: 10.1103/PhysRevB.87.214105 PACS number(s): 66.30.−h

I. INTRODUCTION

Alumina (commonly in the crystal form of α-Al_2O_3), as an important refractory oxide with a large electronic band gap, has relatively high hardness, strength, melting point, wear resistance, and chemical stability. Hence, alumina has been widely employed in such technological applications as the substrate of electronic circuits, the substrate of metallic catalysts, and the container of corrosive chemicals. In particular, the formation of protective α-Al_2O_3 scale is a crucial requirement for high-temperature Al-containing alloys (for instance, FeCrAl and NiCrAl) to resist oxidation under their operating conditions.[1,2] In many cases, the functional performance (such as sintering, creep, and scale growth) of alumina depends strongly on the diffusion processes in its crystalline materials.[3,4] Consequently, the diffusion processes of oxygen (O) anions and aluminum (Al) cations in α-Al_2O_3 have been extensively measured in experiments[5–15] and modeled in simulations.[16–20]

Oxygen diffusion in undoped α-Al_2O_3 single crystals and polycrystals have been measured by several research groups using either secondary ion mass spectroscopy (SIMS) or nuclear reaction analysis (NRA) techniques to determine the ^{18}O depth profiles following high temperature exchange with ^{18}O-enriched oxygen gas. From Arrhenius plots of diffusion coefficient data with respect to reciprocal temperature, the activation energy for O diffusion in α-Al_2O_3 could be obtained in these measurements. The currently available experimental results indicated that the activation energy for O lattice diffusion fell into the range between 531 kJ/mol (i.e. 5.50 eV)[12] and 787 kJ/mol (i.e. 8.15 eV),[7] while the activation energy for O grain boundary diffusion varied from 294 kJ/mol (i.e. 3.05 eV)[9] to 896 kJ/mol (i.e. 9.29 eV).[10] It is notable above that the measured activation energy for O grain boundary diffusion could be even higher than that for O lattice diffusion. Indeed, Prot *et al.* found the activation energy for O lattice diffusion to be 636 kJ/mol (i.e. 6.59 eV), while that for O grain boundary diffusion to be 896 kJ/mol (i.e. 9.29 eV) in their measurement.[10] Moreover, Nakagawa *et al.* reported their measured activation energy for O grain boundary diffusion to be 627 kJ/mol (i.e. 6.50 eV),[13] which was also higher than their own value (531 kJ/mol)[12] for O lattice diffusion. This finding in α-Al_2O_3 is contrary to what is normally found in metals. Furthermore, recent experimental data revealed that the O diffusion coefficients could vary up to 10^3 times along different grain boundaries (GBs) in α-Al_2O_3 and were closely related to the local arrangement of atoms on the GBs.[15] As compared to O diffusion, the experimental studies on Al diffusion in alumina are relatively scarce. So far, there are only two measurements of Al diffusion processes by analyzing the attained profiles of ^{26}Al tracers in undoped α-Al_2O_3 samples at elevated temperatures. It was found that the activation energy for Al diffusion was 477 kJ/mol (i.e. 4.94 eV)[6] in polycrystal alumina and 510 kJ/mol (i.e. 5.29 eV)[8] in single-crystal alumina. These results suggested that the Al lattice diffusion (with activation energy of 5.29 eV) would be faster than the O lattice diffusion (with activation energy of at least 5.50 eV) in α-Al_2O_3. In addition, Ref. 8 reported that the Al grain boundary diffusion could also have higher activation energy [850 kJ/mol (i.e. 8.81 eV)] than the Al lattice diffusion in alumina.

Complementary to experimental measurements, computer simulation techniques have already been employed to elucidate the mechanism of diffusion processes in alumina at an atomistic scale. Jacobs *et al.* calculated the activation energy for O vacancy migration in α-Al_2O_3 lattice to be about 1 to 2.5 eV using both the semiempirical model and pairwise Buckingham empirical potentials.[16] As compared with experimental data (i.e. 5.50 to 8.15 eV), these theoretical predictions were obviously too low. Achieving an improved agreement between theory and experiment, Aschauer *et al.* extracted the activation energy for O lattice diffusion to

be 510.83 kJ/mol (i.e. 5.29 eV) from their empirical pair potential based metadynamics and the kinetic Monte Carlo simulations.[19] Both studies (Refs. 16 and 19) pointed out that there were multiple elementary routes contributing to the overall O diffusion processes in alumina. Regarding the short-circuit diffusion mechanisms in alumina, Harding *et al.*[17] calculated the activation energies for Al vacancy migration along various GBs using the same empirical pair potential employed in Ref. 19. They found that, not only the metal vacancy diffusion behavior varied greatly from one GB to another, but also the individual hops within the same GB differed considerably. Relevantly, Milas *et al.* investigated the diffusion of Al and O atoms on the (0001) surface of α-Al_2O_3 with density functional theory (DFT) calculations.[20] It was predicted that Al surface diffusion would be facile with activation energy of 0.73 eV, but O surface diffusion would involve intermediate metastable state with an overall energy barrier of 1.67 eV.

Although much research has been conducted on the diffusion processes in alumina, there is still a great deal to be understood as related to the mechanism and energetics of Al and O diffusion both in the bulk crystal and on the GBs.[21] In order to gain further insights into various diffusion processes in α-Al_2O_3, in this paper, we used first-principles DFT calculation method to determine the minimum energy paths, configuration of transition states, and activation energies for both O and Al lattice diffusion and grain boundary diffusion via vacancy migration mechanism. In particular, we modeled the O and Al grain boundary diffusion processes in alumina along both low-energy and high-energy representative GBs. In most of previous atomistic simulations,[16,17,19] some kinds of empirical potentials were used when modeling the diffusion processes in alumina. The reliability and accuracy of the predictions from these atomistic simulations strongly depended on the quality of the employed empirical potentials. In contrast, the first-principles DFT calculation has been demonstrated to yield reliable and accurate predictions on various materials properties.[22] Consequently, our first-principles study enables us to reliably elucidate how the local atomic structure of GBs affects the diffusion processes in alumina.

II. COMPUTATIONAL METHOD AND MODELS

The first-principles DFT calculations in this study were performed using the Vienna *Ab initio* Simulation Package (VASP) code.[23,24] In all these calculations, we used projector augmented wave (PAW) method[25] and a kinetic energy cutoff of 500 eV to expand the electronic wave functions in the plane-wave basis. The generalized gradient approximation with Perdew–Burke–Ernzerhof (PBE) functional[26] was used for evaluating exchange-correlation energy. Fully optimized structures of crystal lattice, GBs, and vacancy defects of α-Al_2O_3 were obtained by reducing the Hellman–Feynman force acting on each ion in the corresponding models to less than 0.01 eV/Å. In this study, the activation energy for diffusion processes in α-Al_2O_3 were computed as the energy difference between the transition state and the initial state during a diffusive jump of exchanging the positions of an (O or Al) atom with its neighboring vacancy. The transition state of diffusive jumps was located using the climbing image

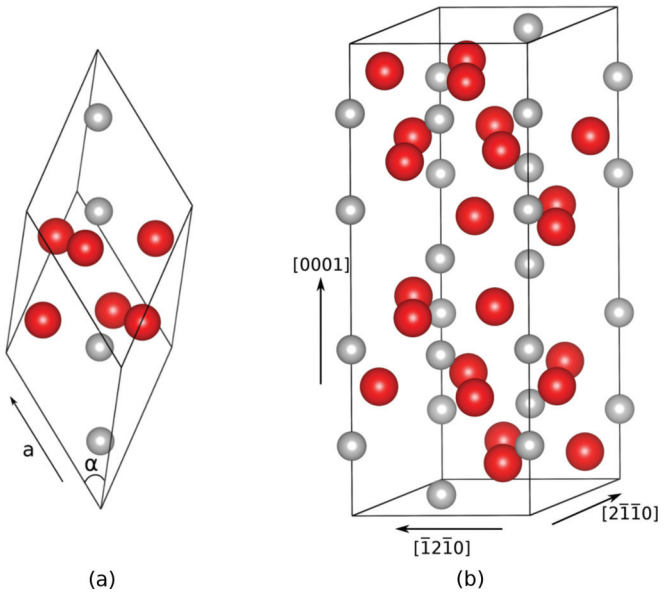

FIG. 1. (Color online) (a) Primitive unit cell and (b) conventional hexagonal unit cell of the crystal structure of α-Al_2O_3. In the figure, gray balls represent Al atoms, and red balls represent O atoms.

nudged elastic band (CI-NEB) method,[27] in which all the force components perpendicular to the tangent of the diffusion pathway were reduced to be less than 0.05 eV/Å.

The crystal structure of α-Al_2O_3 has a space group of $R\bar{3}c$ and contains 10 atoms (4 Al atoms and 6 O atoms) in its primitive unit cell [shown in Fig. 1(a)]. Conventionally, crystal alumina is represented with a hexagonal unit cell [shown in Fig. 1(b)] consisting of 30 atoms (12 Al atoms and 18 O atoms). Lattice diffusions in alumina were simulated in a $2 \times 2 \times 1$ supercell of conventional hexagonal cells. The three axes of the supercell were along [2$\bar{1}\bar{1}$0] (spanning 9.6 Å), [$\bar{1}$2$\bar{1}$0] (spanning 9.6 Å), and [0001] (spanning 13.1 Å) directions. There were in total 120 atoms (48 Al atoms and 72 O atoms) in the simulation cell. We used a $3 \times 3 \times 2$ Monkhorst–Pack k-point mesh[28] for k-space integration in our lattice diffusion calculations.

Modeling GBs of alumina, we placed two crystal grains sharing a boundary plane in a periodic supercell and added a vacuum space along the normal direction of the GB to separate the other ends of the two grains. Specifically, the $\Sigma 3(0001)$ GB of alumina was modeled with a periodic supercell, which contained a 10-Å vacuum space along the [0001] direction and had dimensions of [2$\bar{1}\bar{1}$0] (spanning 9.6 Å) and [$\bar{1}$2$\bar{1}$0] (spanning 4.8 Å) normal to the [0001] (spanning 36.3 Å) direction. There are again 24 (stoichiometric Al_2O_3) units in each supercell. Namely, we have 120 atoms (48 Al atoms and 72 O atoms) in the simulation cell. Hence, the whole supercell of the $\Sigma 3(0001)$ GBs is ensured to have neutral charge. The interphase of the $\Sigma 3(0001)$ GB laid in the middle of the simulation cell and consisted of either 4 Al atoms or 6 O atoms, as shown in Fig. 2. The k-point mesh was set as $2 \times 4 \times 1$ for the DFT calculations of this GB. The $\Sigma 3(10\bar{1}0)$ GB of alumina was modeled with an orthorhombic supercell, which contained a 10-Å vacuum space along the [10$\bar{1}$0] direction and had cell dimensions of [$\bar{1}$2$\bar{1}$0] (spanning 4.8 Å) and [0001] (spanning 13.1 Å) normal to the [10$\bar{1}$0] (spanning 26.7 Å) direction. In

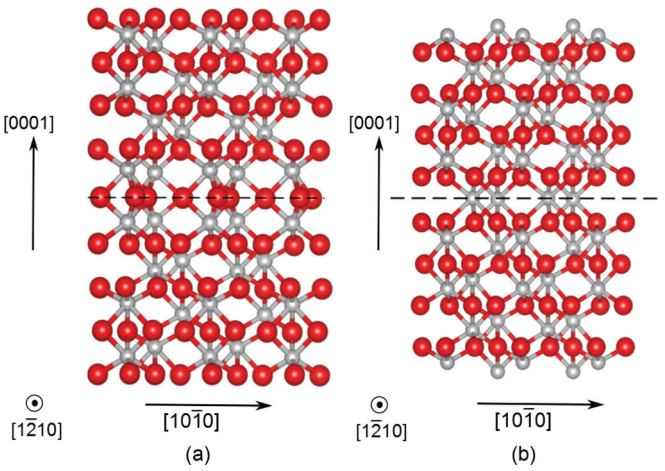

FIG. 2. (Color online) Relaxed atomic structures of high-energy (a) O-terminated and (b) Al-terminated $\Sigma3(0001)$ GBs of α-Al_2O_3. The two structures are shown as the projections on (1$\bar{2}$10) plane. In the figure, gray balls represent Al atoms, red balls represent O atoms, and black dashed lines indicate the interface of the two GBs.

our modeled $\Sigma3(10\bar{1}0)$ GB, there were in total 120 atoms (48 Al atoms and 72 O atoms). The interphase of the $\Sigma3(10\bar{1}0)$ GB laid in the middle of the simulation cell and consisted of 4 Al atoms and 6 O atoms, as shown in Fig. 3. The k-point mesh was set as $5 \times 3 \times 1$ for the DFT calculations of the $\Sigma3(10\bar{1}0)$ GB in this study.

When optimizing the structure of the GBs, we fixed the positions of the atoms in the outermost four layers on both ends of the $\Sigma3(0001)$ GB model and in the outermost three layers on both ends of the $\Sigma3(10\bar{1}0)$ GB model to those in the bulk alumina crystals. All the other atoms in the GBs were allowed to fully relax their positions to reach the lowest energy configuration. Moreover, minimizing the strain on the GB between the two grains, we also extended the models in the direction normal to the GB to find the equilibrium GB structure that had the lowest energy with respect to such expansion. In Supplemental Material,[29] (see also Refs. 30–34, and references therein) we verified the accuracy of our GB simulations by comparing the relaxed structures of the O-terminated $\Sigma3(0001)$ GB attained with our free-surface model and conventional periodic boundary model.

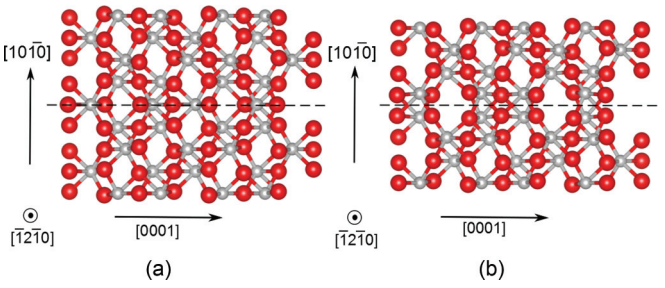

FIG. 3. (Color online) Relaxed atomic structures of low-energy (a) screw-rotation and (b) glide-mirror $\Sigma3(10\bar{1}0)$ GBs of α-Al_2O_3. The two structures are shown as the projections on ($\bar{1}$2$\bar{1}$0) plane. In the figure, gray balls represent Al atoms, red balls represent O atoms, and black dashed lines indicate the interface of the two GBs.

III. OPTIMIZED ATOMISTIC STRUCTURES

A. Bulk α-Al_2O_3

In α-Al_2O_3 crystal (as shown in Fig. 1), O atom occupies a tetrahedral site enclosed by four nearest neighboring Al atoms (denoted as fourfold coordinated) whereas Al atom occupies an octahedral site enclosed by six nearest neighboring O atoms (denoted as sixfold coordinated). It notes that the Al atoms only occupy 2/3 of the possible octahedral sites formed by the O atoms in the lattice of alumina. Our DFT calculations gave the optimized lattice parameters for the hexagonal unit cell of α-Al_2O_3 to be $a = 4.81$ Å and $c = 13.31$ Å, the optimized internal parameter of Al atoms to be $\mu = 0.352$, and the optimized internal parameter of O atoms to be $\nu = 0.306$. Our results in this study are consistent with previous theoretical predictions[35] and experimental measurements.[36]

B. $\Sigma3(0001)$ GB

In this paper, we constructed two (O-terminated and Al-terminated) $\Sigma3(0001)$ basal twin GBs for the purpose of modeling high-energy GBs in α-Al_2O_3. For the O-terminated $\Sigma3(0001)$ GB [Fig. 2(a)], we chose a central O layer as the interphase plane of the GB and arranged the two grains to be mirror-symmetric with respect to this plane. After relaxation, all the O atoms in the interphase of the O-terminated $\Sigma3(0001)$ GB are still fourfold coordinated. The separation between the neighboring Al layers on the two sides of the GB was determined to be 2.53 Å, about 16% larger than the separation of the neighboring Al (0001) layers in bulk alumina. However, the mirror symmetry of the GB caused that the Al atoms above the interphase were right on the top of the Al atoms below the interphase along the [0001] direction. As a result, the Al-Al distance across the GB was 11% smaller than the corresponding value (2.68 Å) in bulk α-Al_2O_3. The formation energy of the O-terminated $\Sigma3(0001)$ GB grain boundary was calculated in this paper to be 2.38 J/m^2, which is consistent with the value of 1.99 J/m^2 from previous DFT calculation.[34]

In Fig. 2(b), we showed the optimized structure of our Al-terminated $\Sigma3(0001)$ GB which has the central Al layer as mirror-symmetric plane. In the interphase of this GB, the Al atoms are still sixfold coordinated. The separation between the neighboring O layers on the two sides of the GB along the [0001] direction was determined to be 2.42 Å, which is 11% larger than the separation (2.19 Å) between two adjacent O (0001) layers in bulk α-Al_2O_3. After relaxation, the O-O distance across the GB was reduced by about 5% compared to the corresponding value (2.55 Å) in bulk α-Al_2O_3. We calculated the formation energy of this Al-terminated $\Sigma3(0001)$ GB to be 2.12 J/m^2. It should be noted that our thus-modeled Al-terminated $\Sigma3(0001)$ GB is not the lowest energy configuration of the $\Sigma3(0001)$ GB as illustrated in previous experiments[37] and computations.[34] Rotating the upper half of the crystal by 180° along [0001] axis would convert our modeled Al-terminated $\Sigma3(0001)$ GB to the lowest-energy $\Sigma3(0001)$ GB, which was predicted to have quite low formation energy of about 0.73 J/m^2.[34] In this theoretical paper, we are interested in investigating how the atoms diffuse along high-energy GBs of α-Al_2O_3. Consequently, we constructed

the two $\Sigma 3(0001)$ GBs (O-terminated and Al-terminated) with relatively high formation energy (about 2 J/m^2).

C. $\Sigma 3(10\bar{1}0)$ GB

In this paper, we constructed two (screw-rotation and glide-mirror) $\Sigma 3(10\bar{1}0)$ twin GBs for the purpose of modeling low-energy GBs of α-Al_2O_3. For these two GBs, we followed the same construction procedures as suggested in Ref. 38. First, we rotated the upper half of the modeled alumina crystal by 180° around $[10\bar{1}0]$ with respect to the bottom half of the crystal, which was oriented along $[10\bar{1}0]$ direction. Then, we translated the upper half of the crystal by a vector of $\frac{1}{2}[\bar{1}2\bar{1}0] + \frac{1}{3}[0001]$ parallel to $(10\bar{1}0)$ to attain the screw-rotation $\Sigma 3(10\bar{1}0)$ GB and by a vector of $\frac{1}{2}[\bar{1}2\bar{1}0]$ parallel to $(10\bar{1}0)$ to attain the glide-mirror $\Sigma 3(10\bar{1}0)$ GB. Figure 3 shows the optimized structures of these two GBs from our DFT calculations.

It could be seen in Fig. 3 that the interphase of the screw-rotation $\Sigma 3(10\bar{1}0)$ GB was a single atomic layer composed of both Al and O atoms, whereas the interphase of the glide-mirror $\Sigma 3(10\bar{1}0)$ GB consisted of two atomic layers. Moreover, it was observed that all the Al atoms in the interphase of these two GBs were still sixfold coordinated. However, the O atoms on the GBs could be threefold coordinated (undercoordinated as compared with those in bulk crystal), fourfold coordinated (same as those in bulk crystal), or fivefold coordinated (overcoordinated as compared with those in bulk crystal). After structural relaxation, the separation of the adjacent $(10\bar{1}0)$ layers on the screw-rotation GB became 1.42 Å, which is only slightly larger than the corresponding bulk value (1.39 Å), and the separation of the adjacent $(10\bar{1}0)$ layers on the glide-mirror GB became 1.59 Å, which is about 14% larger than the corresponding bulk value of α-Al_2O_3.

Our DFT calculation predicted the formation energy of the screw-rotation $\Sigma 3(10\bar{1}0)$ GB to be 0.25 J/m^2 and the formation energy of the glide-mirror $\Sigma 3(10\bar{1}0)$ GB to be 0.39 J/m^2. Consequently, we used these two $\Sigma 3(10\bar{1}0)$ GBs representing low-energy GBs of α-Al_2O_3 in this study.

D. Local atomic structures

It has been well-recognized that the energetics of atomic diffusion processes is closely related to local atomic structures. To elaborate how the grain boundary diffusion differs from the lattice diffusion, we first examined how the local atomic structures of the modeled GBs differ from those in bulk alumina crystal. In bulk α-Al_2O_3 [shown in Fig. 4(a)], the O atom lies at the center of a tetrahedron whose four vertices are Al atoms, and the Al atom lies at the center of an octahedron whose six vertices are occupied by O atoms. It notes that the distance between the central O (or Al) atoms to their neighboring Al (or O) atoms are not always equal in alumina crystal. Our DFT calculations showed that half of the Al-O bonds have bond length of 1.87 Å, and the other half have slightly longer bond length of 1.99 Å in α-Al_2O_3. Moreover, the adjacent Al-O bonds form an angle of about 110° around the O atom and form an angle of about 90° around the Al atom.

In the interphase of O-terminated $\Sigma 3(0001)$ GB [Fig. 2(a)], every O atom is still surrounded by four Al atoms. However, as shown in Fig. 4(b), these four Al atoms constitute a planar

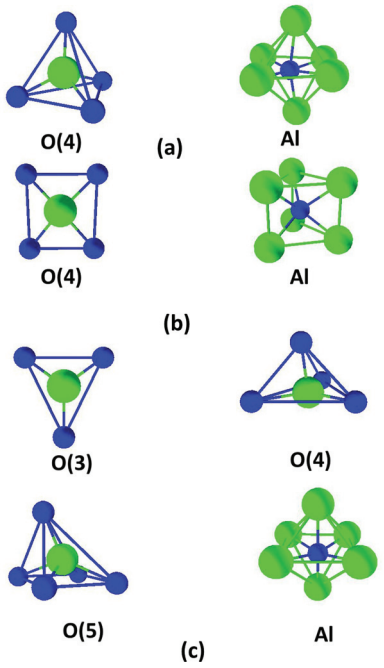

FIG. 4. (Color online) Local atomic structures showing the relative positions of the central O (or Al) lattice site and its nearest-neighboring Al (or O) lattice sites in the relaxed (a) bulk α-Al_2O_3, (b) the interphase of $\Sigma 3(0001)$ GBs, and (c) the interphase of $\Sigma 3(10\bar{1}0)$ GBs. In the figure, blue balls represent Al lattice sites, and green balls represent O lattice sites.

tetragon instead of a tetrahedron, and the O atom is located above the center of the Al plane by about 0.35 Å. In this configuration, the four Al-O bonds have the lengths ranging from 1.85 to 1.98 Å, which are similar to those in bulk alumina. However, the angles between two adjacent Al-O bonds are averaged to be about 88°, which is significantly smaller than the corresponding bulk value. Moreover, Fig. 4(b) showed that, in the interphase of Al-terminated $\Sigma 3(0001)$ GB [Fig. 2(b)], the Al atom sits in the center of a triangular prism whose six vertices are occupied by O atoms. Our further analysis revealed that, although both are sixfold coordinated, there were two distinct types of Al atoms in the Al-terminated $\Sigma 3(0001)$ GB. With the surrounding six O atoms, atom "Al_A" would form three Al-O bonds with length of 1.91 Å and another three Al-O bonds with length of 1.93 Å. In contrast, atom "Al_B" would have three Al-O bonds with length of 1.99 Å and the other three Al-O bonds with length of 2.08 Å. It is noticeable that the atoms have the same coordination numbers but different local atomic configurations in the $\Sigma 3(0001)$ GBs and in the bulk alumina. Thus, our DFT results suggested that the local atomic configurations with unfavorable Al-O bond angles are responsible for the high formation energies of the modeled $\Sigma 3(0001)$ GBs.

In the interphase of the two $\Sigma 3(10\bar{1}0)$ GBs, the O atoms could have coordination number of three [denoted as "O(3)"], four [denoted as "O(4)"], or five [denoted as "O(5)"], and all the Al atoms have coordination number of six. In Fig. 4(c), we plotted the local atomic structures of these O atoms and Al atoms in the interphase of the GBs. Figure 4(c) showed that atom O(3) laid at the center of a triangle, atom O(4) laid

close to the center of a tetrahedron, atom O(5) laid at the center of a pentahedron, and Al atom laid at the center of an octahedron. Our DFT results also revealed that the three Al-O bonds between O(3) and its neighboring Al atoms were slightly shorter than the Al-O bonds in bulk crystal, the four Al-O bonds between O(4) and its neighboring Al atoms had the exactly same length as those in bulk crystal, and only two of the five Al-O bonds between O(5) and its neighboring Al atoms were about 9% longer than the Al-O bonds in bulk crystal. Although the O atoms in the GB have different numbers of neighboring Al atoms, the adjacent Al-O bonds form an angle [about 118° around atom O(3), about 106° around atom O(4), and about 97° around atom O(5)] not very different from the Al-O angle of 110° around the O atoms in α-Al_2O_3 crystal. As mentioned in literature,[38] the Al atoms in the $\Sigma3(10\bar{1}0)$ GBs have two distinct local atomic structures (denoted as "Al_A" and "Al_B") which differ mainly in the lengths of the six Al-O bonds. It appears that maintaining the bulklike Al-O bond angles in the $\Sigma3(10\bar{1}0)$ GBs leads to the low formation energy of these two GBs.

IV. VACANCY FORMATION ENERGY

The formation energies of various neutral and charged defects in alumina had been extensively studied using the DFT computation method.[39–42] In this paper, we studied the formation energies, relaxed structures, and mobility of the vacancies with neutral charge state in the bulk region and representative grain boundaries of alumina. For atomic vacancy, the formation energy is normally evaluated as the energy difference between the model system containing a vacancy and the otherwise perfect system, and further plus the chemical potential of the atomic species. It has been recognized that the different choices of the O and Al chemical potentials largely accounted for the discrepancy in the reported values of the same vacancy defect formation energy. In this paper, we chose simply one half of the potential energy of a gas O_2 molecule as the chemical potential of element O when calculating O vacancy formation energies and the atomic energy of metal Al as the chemical potential of element Al when calculating Al vacancy formation energies. We listed in Tables I and II the calculated formation energies of O and Al vacancies in the bulk lattice and various GBs of α-Al_2O_3. More relevant to this paper, we also gave in Tables I and II the energy difference for a vacancy to lie in the GBs relative to lie in the bulk crystal. Negative signs of such energy difference imply that the vacancies energetically prefer segregating to the GB than staying inside a grain.

TABLE I. Calculated formation energy (E_f) of an O vacancy in the bulk crystal, O-terminated $\Sigma3(0001)$ GB, screw-rotation $\Sigma3(10\bar{1}0)$ GB, and glide-mirror $\Sigma3(10\bar{1}0)$ GB of α-Al_2O_3. For comparison, relative O vacancy formation energies (ΔE_f) with respect to that in bulk α-Al_2O_3 crystal are also included in the table.

		E_f (eV)	ΔE_f (eV)
Bulk crystal	O(4)	6.80	0.00
O-terminated $\Sigma3(0001)$ GB	O(4)	5.43	−1.37
Screw-rotation $\Sigma3(10\bar{1}0)$ GB	O(3)	6.42	−0.38
	O(4)	6.53	−0.27
	O(5)	6.60	−0.20
Glide-mirror $\Sigma3(10\bar{1}0)$ GB	O(3)	6.42	−0.38
	O(4)	6.64	−0.16
	O(5)	6.60	−0.20

TABLE II. Calculated formation energy (E_f) of an Al vacancy in the bulk crystal, Al-terminated $\Sigma3(0001)$ GB, screw-rotation $\Sigma3(10\bar{1}0)$ GB, and glide-mirror $\Sigma3(10\bar{1}0)$ GB of α-Al_2O_3. For comparison, relative Al vacancy formation energies (ΔE_f) with respect to that in bulk α-Al_2O_3 crystal are also included in the table.

		E_f (eV)	ΔE_f (eV)
Bulk crystal	Al	12.13	0.00
Al-terminated $\Sigma3(0001)$ GB	Al_A	8.74	−3.39
	Al_B	9.32	−2.81
Screw-rotation $\Sigma3(10\bar{1}0)$ GB	Al_A	11.61	−0.52
	Al_B	12.21	0.08
Glide-mirror $\Sigma3(10\bar{1}0)$ GB	Al_A	11.18	−0.95
	Al_B	11.75	−0.38

Our DFT calculation predicted the formation energies of O and Al vacancies to be 6.80 and 12.13 eV in bulk alumina, respectively. As compared with our calculated value for O vacancy in bulk crystal, the O vacancy formation energies in the high-energy O-terminated $\Sigma3(0001)$ GB were found to be at least 1.37 eV lower, whereas the O vacancy formation energies in the low-energy $\Sigma3(10\bar{1}0)$ GBs were found to be merely about 0.27 eV lower on average. Similarly, we noticed that the Al vacancy formation energies in the high-energy Al-terminated $\Sigma3(0001)$ GB were at least 2.81 eV lower than the value in bulk alumina, whereas the Al vacancy formation energies in the low-energy $\Sigma3(10\bar{1}0)$ GBs could just be 0.95 eV lower than the bulk Al vacancy formation energy. Consequently, our results in Tables I and II indicate that the O and Al vacancies in α-Al_2O_3 tended to segregate to the GBs from the bulk crystal, and the segregation tendency was related to the formation energy of the GBs (the higher the GB formation energy, the lower the vacancy formation energy).

It has been revealed in previous atomistic simulations[43–45] that the vacancy at the GB of metals could often induce relatively large atomic displacements in its surrounding region (namely, vacancy delocalization) and thus possibly reduce the activation energy for diffusion at the GBs. In this paper, we examined all the relaxed structures of the vacancies at our modeled GBs of α-Al_2O_3 and found in all the cases that the atomic displacements around a vacancy were constricted to the immediate vicinity of the vacancy. Moreover, all the resultant displacements of atoms were less 5% of the equilibrium length of Al-O bonds. Therefore, we did not observe the vacancy delocalization phenomenon at the $\Sigma3(0001)$ and $\Sigma3(10\bar{1}0)$ GBs of α-Al_2O_3 in this study.

V. ATOMIC DIFFUSION

A. Lattice diffusion in bulk α-Al_2O_3

Referencing to the equilibrium structure of α-Al_2O_3 crystal (shown in Fig. 1), we identified multiple elementary diffusive

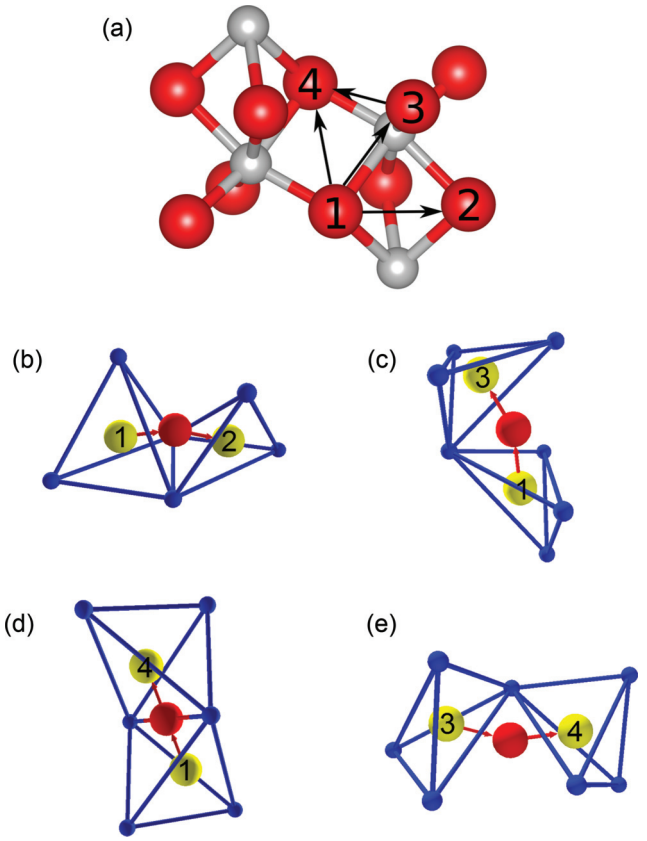

FIG. 5. (Color online) (a) Schematics of four elementary O diffusive jumps in bulk α-Al_2O_3 on the $(1\bar{2}10)$ projection of the crystal lattice. In the figure, gray balls represent Al atoms, red balls represent O atoms, and black arrows delineate various vacancy-O atom exchange. Local atomic structures of the migrating O atom are depicted in (b) for jump O_1-O_2, in (c) for jump O_1-O_3, in (d) for jump O_1-O_4, and in (e) for jump O_3-O_4. In (b)–(e), yellow balls are used to mark the initial and final positions of the migrating O atom, red balls mark the location of the migrating O atom in the transition states, red arrows indicate the direction of the diffusive jumps, and blue balls represent surrounding Al lattice sites.

jumps for O and Al atoms to diffuse in bulk alumina through vacancy-atom exchange mechanism. As shown in Fig. 5(a), there are two types of O elementary diffusive jumps (jump O_1-O_2 and jump O_3-O_4) in the (0001) plane and two types of elementary diffusive jumps (jump O_1-O_3 and jump O_1-O_4) connecting the two (0001) planes (i.e. along the [0001] direction). All the other long-range diffusive paths for an O atom in alumina can be attained by combining these four elementary jumps. Here, our analysis of the existence of the multiple O vacancy diffusive jumps agrees well with the simulation results from metadynamics calculations.[19] For each of these O elementary diffusive jumps, we used the CI-NEB method to determine the minimum energy path and the transition state for an O atom to migrate from one position to the other. We report in Table III our calculated activation energies for the O lattice diffusion through these four possible diffusive jumps. We predicted that jump O_1-O_2 (which has the smallest diffusion distance) required activation energy of 3.58 eV, very close to the value of 3.7 eV calculated in Ref. 18 for the same jump. However, it is worth mentioning that these

TABLE III. Predicted diffusion distances and activation energies of the elementary O and Al diffusive jumps in bulk α-Al_2O_3 lattice. The four elementary O diffusive jumps (O_1-O_2, O_1-O_3, O_1-O_4, and O_3-O_4) are graphically shown in Fig. 5(a) and the four elementary Al diffusive jumps (Al_1-Al_2, Al_1-Al_3, Al_3-Al_4, and Al_2-Al_4) are graphically shown in Fig. 6(a).

Diffusive jumps	Diffusion distance (Å)	Activation energy (eV)
	O lattice diffusion	
O_1-O_2	2.55	3.58
O_1-O_3	2.75	4.11
O_1-O_4	2.65	4.67
O_3-O_4	2.89	5.03
	Al lattice diffusion	
Al_1-Al_2	2.82	1.80
Al_1-Al_3	2.68	2.05
Al_3-Al_4	3.25	2.25
Al_2-Al_4	3.88	3.17

low activation energy O_1-O_2 jumps are spatially limited within a small region in the (0001) plane of α-Al_2O_3 and cannot constitute long-range diffusion paths only by themselves. Moreover, our results in Table III indicate the activation energy for O_3-O_4 lattice diffusive jump [which is extendable to the whole (0001) plane] to be 5.03 eV, which is the comparable to the experimental data in Ref. 12 for O lattice diffusion in α-Al_2O_3. It is also noticeable that our calculated activation energy is not well correlated with the distance of the diffusive jump.

Furthermore, we plotted in Figs. 5(b)–5(e) the minimum energy path (marked in arrows) and transition state (denoted with a red ball) of O lattice diffusion along the four elementary diffusive jumps, respectively. In all the starting and ending positions of the four jumps, the O atom has four nearest neighboring Al atoms and thus is fourfold coordinated. However, our DFT calculations revealed that the migrating O atom would be fourfold coordinated in the transition state of jump O_1-O_2, threefold coordinated in the transition state of jump O_1-O_3, twofold coordinated in the transition state of jump O_1-O_4, and twofold coordinated in the transition state of jump O_3-O_4. It appears in our DFT results that the coordination number of the migrating O atom in the transition state is correlated with the calculated activation energy of the diffusive jumps. Namely, the higher the coordination number of O in the transition state, the lower the activation energy of the diffusive jump.

For Al lattice diffusion in α-Al_2O_3, we conducted our DFT calculations for the following four elementary diffusive jumps as shown in Fig. 6(a): jump Al_1-Al_2 is a jump between the two Al atoms locating in the two neighboring (0001) layers; jump Al_1-Al_3 is a jump along [0001] direction between the two Al atoms locating in the (0001) layers separated by one O layer; jump Al_3-Al_4 is a jump tilted away from [0001] direction and between the two Al atoms locating in the (0001) layers separated by one O layer; and jump Al_2-Al_4 is a jump along [0001] direction between the two Al atoms locating in the (0001) layers separated by two O layers. Table III gave the calculated activation energies for these Al lattice diffusion jumps and

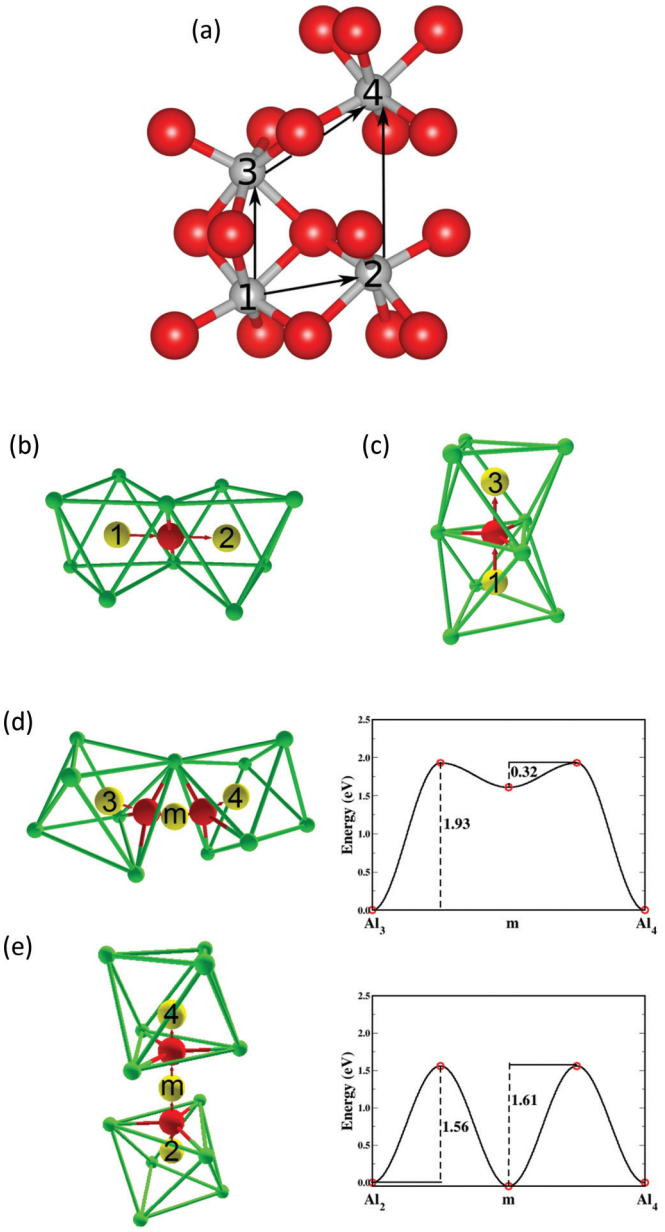

FIG. 6. (Color online) (a) Schematics of four elementary Al diffusive jumps in bulk α-Al_2O_3 on the $(1\bar{2}10)$ projection of the crystal lattice. In the figure, gray balls represent Al atoms, red balls represent O atoms, and black arrows delineate various vacancy-Al atom exchange paths. Local atomic structures of the migrating Al atom are depicted in (b) for jump Al_1-Al_2, in (c) for jump Al_1-Al_3, in (d) for jump Al_3-Al_4, and in (e) for jump Al_2-Al_4. In (b)–(e), yellow balls are used to mark the initial, intermediate (marked with symbol "m"), and final positions of the migrating Al atom, red balls mark the location of the migrating Al atom in the transition states, and red arrows indicate the direction of the diffusive jumps, green balls represent surrounding O lattice sites. Also, we plotted in (d) and (e) our calculated minimum energy path for the Al atom diffusion through jumps Al_3-Al_4 and Al_2-Al_4, respectively.

Figs. 6(b)–6(e) presented the minimum energy pathway of the four Al elementary diffusive jumps, respectively.

It was found for jump Al_1-Al_2 that, in the transition state, the migrating Al atom was located at the middle point of the edge shared by the two O octahedrons surrounding the initial and final Al positions, and the activation energy was 1.80 eV. In contrast, in the transition state of jump Al_1-Al_3, the migrating Al atom was located at the center of the triangular facet shared by the two O octahedrons surrounding the initial and final Al positions. The activation energy for this jump was predicted to be 2.05 eV. Our DFT calculations indicated that both Al_1-Al_2 and Al_1-Al_3 diffusive jumps could be completed with one simple jump of Al atom from the starting position to the final position. However, jumps Al_2-Al_4 and Al_3-Al_4 involved an intermediate stable position and two simple jumps. Figures 6(d) and 6(e) showed the minimum energy path of jump Al_3-Al_4 and Al_2-Al_4, respectively. It could be seen in the figures that there was a locally minimum-energy position (marked as "m") between the two facing triangular facets of the two O octahedrons for the migrating Al atom to stay. Consequently, it involved two simple jumps [Al_3-m (or Al_2-m) and m-Al_4], whose transition state was the migrating Al atom lying at the center of the triangular facet of the O octahedron, to complete these two jumps. Along the minimum energy path of jump Al_3-Al_4 [Fig. 6(d)], we found that the activation energy of the Al_3-m jump was 1.93 eV, and the activation energy of the m-Al_4 jump was 0.32 eV. Thus, it requires overall activation energy of 2.25 eV to complete jump Al_3-Al_4 in bulk α-Al_2O_3. Similarly, our DFT calculations predicted the overall activation energy of 3.17 eV (1.56 eV for the Al_2-m jump and 1.61 eV for the m-Al_4 jump) for the complete jump Al_2-Al_4. Compared with the experimental data of 4.94 eV,[6] our theoretical predictions for the activation energy of Al lattice diffusion in α-Al_2O_3 are more than 1.77 eV lower. This apparent discrepancy between theory and experiments might suggest the existence of other high-energy jumps [for example, jumps from the locally minimum-energy positions in Figs. 6(d) and 6(e) to other Al positions] in the experimental samples.

B. Grain boundary diffusion in Σ3(0001) GB

On the O-terminated Σ3(0001) GB, there are only O lattice sites in the interphase. Although the O vacancy formation energies are same at the various O lattice sites of the GB, two possible elementary diffusive jump paths [jump O_1-O_2 and jump O_1-O_3, as shown in Fig. 7(a)] exist in the (0001) plane. The main difference between the two jumps is diffusion distance: 2.51 Å for jump O_1-O_2 and 2.45 Å for jump O_1-O_3. Given in Table IV, the activation energy of jump O_1-O_2 was calculated to be 1.26 eV and the activation energy of jump O_1-O_3 to be 1.29 eV. Compared with the O lattice diffusion in (0001) plane (jumps O_1-O_2 and O_1-O_3 in Table III), the O grain boundary diffusion along the O-terminated Σ3(0001) GB was predicted to require much lower activation energy (at least by 2.29 eV). Close examination on the local structures along the two diffusive jumps [Fig. 7(c)] revealed that the migrating O atom was fourfold coordinated at the starting and final states but had only two nearest-neighboring Al atoms at the transition states along the minimum-energy diffusion pathways. At the transition states, the angle of Al-O-Al was found to be 95° for jump O_1-O_2 and 107° for jump O_1-O_3.

As pointed out in Table II, there are two types of Al lattice sites with different vacancy formation energies in the interphase of Al-terminated Σ3(0001) GB. Consequently,

TABLE IV. Predicted diffusion distances and activation energies of the elementary O and Al diffusive jumps on the high-energy O-terminated Σ3(0001) GB and Al-terminated Σ3(0001) GB of α-Al_2O_3. The elementary O diffusive jumps (O_1-O_2 and O_1-O_3) on the O-terminated Σ3(0001) GB are graphically shown in Fig. 7(a) and the elementary Al diffusive jumps (Al_1-Al_2 and Al_2-Al_1) on the Al-terminated Σ3(0001) GB are graphically shown in Fig. 7(b).

Diffusive jumps	Diffusion distance (Å)	Activation energy (eV)
O diffusion on O-terminated Σ3(0001) GB		
O_1-O_2	2.51	1.26
O_1-O_3	2.45	1.29
Al diffusion on Al-terminated Σ3(0001) GB		
Al_1-Al_2	2.77	0.64
Al_2-Al_1	2.77	1.22

there are two elementary diffusive jumps [jump Al_1-Al_2 and jump Al_2-Al_1, as shown in Fig. 7(b)] for an Al atom migrating in the (0001) interphase plane of the Al-terminated Σ3(0001) GB. Here, lattice site Al_1, which has higher vacancy formation energy than Al_2, refers to the same atom Al_B in Table II. Table IV reports that our calculated activation energy for diffusive jumps Al_1-Al_2 and Al_2-Al_1 was 0.64 and 1.22 eV, respectively. Thus, the Al grain boundary diffusion in the Al-terminated Σ3(0001) GB requires an average of 0.93 eV for an elementary diffusion step. In contrast, lattice diffusive jump Al_1-Al_2 in bulk α-Al_2O_3 corresponds to the diffusion process in the (0001) plane and has activation energy of 1.80 eV. In Fig. 7(d), the minimum-energy diffusion path of jump Al_1-Al_2 in the Al-terminated Σ3(0001) GB was depicted. As shown in this figure, the migrating Al atom was sixfold coordinated at the starting and final states of the diffusion jump but occupied the center of an O-rectangular facet (i.e. fourfold coordinated) at the transition state of the diffusion.

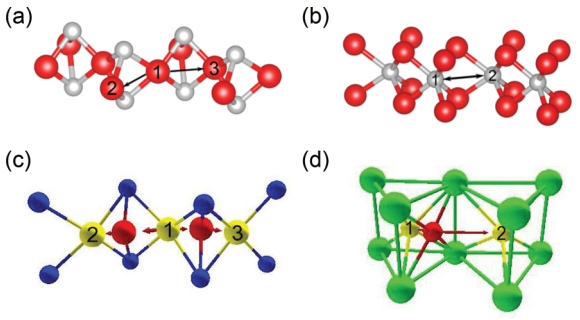

FIG. 7. (Color online) (a) Schematics of two elementary O diffusive jumps in the O-terminated Σ3(0001) GB and (b) schematics of elementary Al diffusive jumps in the Al-terminated Σ3(0001) GB of α-Al_2O_3. In (a), (b), gray balls represent Al atoms, red balls represent O atoms, and black arrows indicate vacancy-atom exchange paths. (c) Local atomic structure of the migrating O atom in O-terminated Σ3(0001) GB and (d) local atomic structure of the migrating Al atom in Al-terminated Σ3(0001) GB. In (c), (d), yellow balls are used to mark the initial and final positions of the migrating atom, red balls show the location of the migrating atom in the transition states, and red arrows indicate the direction of the diffusive jumps, blue balls represent surrounding Al lattice sites in (c), and green balls represent surrounding O lattice sites in (d).

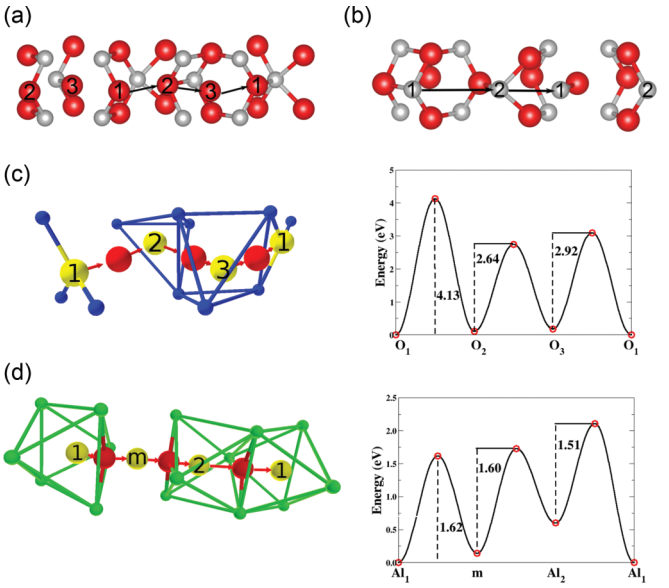

FIG. 8. (Color online) Schematics of a sequence of elementary diffusive jumps for (a) O atom and (b) Al atoms in the screw-rotation Σ3(10$\bar{1}$0) GB of α-Al_2O_3. In (a), (b), gray balls represent Al atoms, red balls represent O atoms, and black arrows indicate vacancy-atom exchange paths. Local atomic structure of (c) migrating O atom and (d) migrating Al atom in the interphase of the screw-rotation Σ3(10$\bar{1}$0) GB following the indicated diffusion paths. In (c), (d), yellow balls are used to mark the initial, intermediate (marked with symbol "m"), and final positions of the migrating atom, red balls mark the location of the migrating atom in the transition states, and red arrows indicate the direction of diffusive jumps, blue balls represent surrounding Al lattice sites in (c), and green balls represent surrounding O lattice sites in (d). Moreover, we plotted in (c) and (d) the calculated minimum energy path for the O atom and Al atom grain boundary diffusion along the indicated diffusion routes, respectively.

C. Grain boundary diffusion in Σ3(10$\bar{1}$0) GB

In the interphase of Σ3(10$\bar{1}$0) GBs, there are both O and Al lattice sites on the (10$\bar{1}$0) plane. Shown in Tables I and II for Σ3(10$\bar{1}$0) GBs, the threefold, fourfold, and fivefold coordinated O vacancies have distinct formation energies, and the two sixfold coordinated Al vacancies also have different formation energies. Hence, the diffusion processes in the interphase of Σ3(10$\bar{1}$0) GBs are considerably complicated as compared to those in the Σ3(0001) GBs. In this paper, we focused our study on the sequential elementary diffusions of O and Al atoms along [0001] direction within the (10$\bar{1}$0) interphase plane of the Σ3(10$\bar{1}$0) GBs. In Figs. 8(a) and 8(b), we plotted three elementary diffusive jumps for O atom (O_1-O_2, O_2-O_3, and O_3-O_1) and two elementary diffusive jumps for Al atom (Al_1-Al_2 and Al_2-Al_1) in the screw-rotation Σ3(10$\bar{1}$0) GB, respectively. Similar plots for the diffusive jumps in the glide-mirror Σ3(10$\bar{1}$0) GB are depicted in Figs. 9(a) and 9(b). Moreover, we gave in Table V the calculated activation energies for these elementary diffusive jumps along the directions as drawn in the figures as well as along the reversing directions.

Furthermore, the local atomic structures and the corresponding energy profiles of the various O elementary diffusion jumps in the screw-rotation Σ3(10$\bar{1}$0) GB were shown in

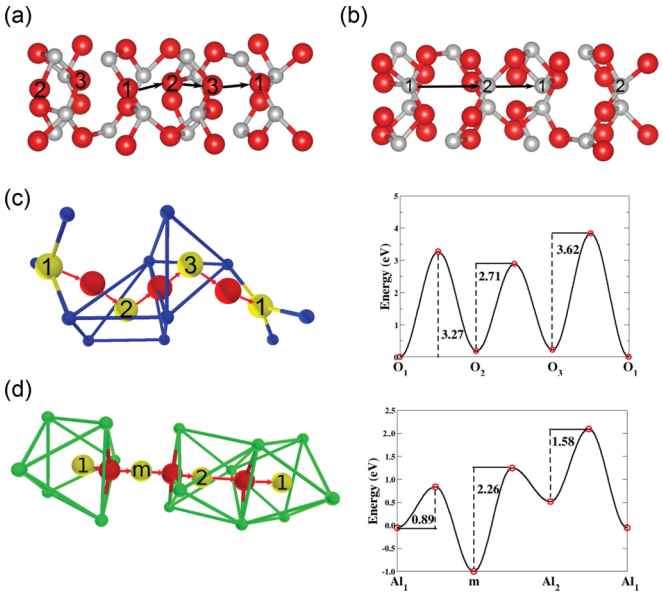

FIG. 9. (Color online) Schematics of a sequence of elementary diffusive jumps for (a) O atom and (b) Al atoms in the glide-mirror $\Sigma3(10\bar{1}0)$ GB of α-Al_2O_3. In (a), (b), gray balls represent Al atoms, red balls represent O atoms, and black arrows indicate vacancy-atom exchange paths. Local atomic structure of (c) migrating O atom and (d) migrating Al atom in the interphase of the glide-mirror $\Sigma3(10\bar{1}0)$ GB following the indicated diffusion paths. In (c), (d), yellow balls are used to mark the initial, intermediate (marked with symbol "m"), and final positions of the migrating atom, red balls mark the location of the migrating atom in the transition states, and red arrows indicate the direction of diffusive jumps, blue balls represent surrounding Al lattice sites in (c), and green balls represent surrounding O lattice sites in (d). Moreover, we plotted in (c) and (d) the calculated minimum energy path for the O atom and Al atom grain boundary diffusion along the indicated diffusion routes, respectively.

Fig. 8(c) and those in the glide-mirror $\Sigma3(10\bar{1}0)$ GB were shown in Fig. 9(c). In Figs. 8(a) and 8(c) for the screw-rotation $\Sigma3(10\bar{1}0)$ GB, it can be discerned that atom O_1 is threefold coordinated, atom O_2 is fourfold coordinated, and atom O_3 is fivefold coordinated. Moreover, Fig. 8(c) showed that the migrating O atom was fourfold coordinated at the transition state of jump O_1-O_2, threefold coordinated at the transition state of jump O_2-O_3, and twofold coordinated at the transition state of jump O_3-O_1. In contrast, atom O_1 is threefold coordinated, atom O_2 is fivefold coordinated, and atom O_3 is fourfold coordinated on the glide-mirror $\Sigma3(10\bar{1}0)$ GB shown in Figs. 9(a) and 9(c). Local atomic structures in Fig. 9(c) showed that the migrating O atom was threefold coordinated at all the transition states of jumps O_1-O_2, O_2-O_3, and O_3-O_1. Among all the studied O elementary jumps in the screw-rotation $\Sigma3(10\bar{1}0)$ GB interphase, jump O_1-O_2 was found to have the highest activation energy of 4.13 eV. Among all the studied O elementary jumps on the glide-mirror $\Sigma3(10\bar{1}0)$ GB interphase, jump O_3-O_1 was found to have the highest activation energy of 3.84 eV. In comparison, the O diffusive jumps in bulk α-Al_2O_3 along [0001] were calculated to be 4.11 eV for jump O_1-O_3 and 4.67 eV for jump O_1-O_4. Hence, our DFT results indicated that the activation energy

TABLE V. Predicted diffusion distances and activation energies (both forward jump and backward jump) of elementary O and Al diffusive jumps on the low-energy screw-rotation $\Sigma3(10\bar{1}0)$ GB and glide-mirror $\Sigma3(10\bar{1}0)$ GB of α-Al_2O_3. The elementary O diffusive jumps (O_1-O_2, O_2-O_3, and O_3-O_1) are graphically shown in Fig. 8(a) for those on the screw-rotation $\Sigma3(10\bar{1}0)$ GB and Fig. 9(a) for those on the glide-mirror $\Sigma3(10\bar{1}0)$ GB. The elementary Al diffusive jumps (Al_1-Al_2, and Al_2-Al_1) are graphically shown in Fig. 8(b) for those on the screw-rotation $\Sigma3(10\bar{1}0)$ GB and Fig. 9(b) for those on the glide-mirror $\Sigma3(10\bar{1}0)$ GB.

Diffusive jumps	Diffusion distance (Å)	Activation energy (eV) (forward jump)	Activation energy (eV) (backward jump)
O diffusion on screw-rotation $\Sigma3(10\bar{1}0)$ GB			
O_1-O_2	2.84	4.13	4.02
O_2-O_3	2.63	2.64	2.57
O_3-O_1	2.70	2.92	3.10
O diffusion on glide-mirror $\Sigma3(10\bar{1}0)$ GB			
O_1-O_2	2.76	3.27	3.09
O_1-O_3	2.60	2.71	2.67
O_1-O_3	2.78	3.62	3.84
Al diffusion on screw-rotation $\Sigma3(10\bar{1}0)$ GB			
Al_1-Al_2	3.86	3.22	2.62
Al_2-Al_1	2.71	1.51	2.11
Al diffusion on glide-mirror $\Sigma3(10\bar{1}0)$ GB			
Al_1-Al_2	3.86	3.15	2.57
Al_2-Al_1	2.71	1.58	2.15

of the O diffusive jumps were quite close in the low-energy $\Sigma3(10\bar{1}0)$ GBs and in bulk crystal of α-Al_2O_3.

The Al diffusive jumps along [0001] in the interphase of the screw-rotation and glide-mirror $\Sigma3(10\bar{1}0)$ GBs are quite similar: one long jump (Al_1-Al_2) and one short jump (Al_2-Al_1) as plotted in Figs. 8(b) and 9(b). As shown in Figs. 8(d) and 9(d), there exists an intermediate stable position (marked as "m") in the route of diffusive jump Al_2-Al_1 and in all the transition states the migrating Al atoms are located at the center of the triangles formed by three O atoms. Comparing the local atomic structures of the migrating Al atoms in $\Sigma3(10\bar{1}0)$ GBs [Figs. 8(d) and 9(d)] and in bulk crystal [Figs. 6(c) and 6(e)], we found that the long diffusive jump Al_1-Al_2 in the GBs [marked in Figs. 8(b) and 9(b)] was comparable to the diffusive jump Al_2-Al_4 in the bulk crystal, whereas the short diffusive jump Al_2-Al_1 in the GBs was comparable to the diffusive jump Al_1-Al_3 in the bulk crystal. Our DFT calculations predicted that the migrating Al atom would first overcome an energy barrier of 1.62 eV (or 0.89 eV) and then another energy barrier of 1.60 eV (or 2.26 eV) along the long diffusive jump Al_1-Al_2 in the screw-rotation (or glide-mirror) $\Sigma3(10\bar{1}0)$ GB. In contrast, the migrating Al atom would first overcome an energy barrier of 1.56 eV and then another energy barrier of 1.61 eV during diffusive jump Al_2-Al_4 in the bulk α-Al_2O_3. Moreover, the activation energy along the reverse direction of the short diffusive jump Al_2-Al_1 was determined to be 2.11 and 2.15 eV in the screw-rotation and glide-mirror $\Sigma3(10\bar{1}0)$ GB, respectively. The corresponding jump Al_1-Al_3 in the bulk crystal only had activation energy of 2.05 eV. Consequently, our results showed that Al diffusion in the $\Sigma3(10\bar{1}0)$ GBs

required even higher activation energy than that in the bulk crystal of α-Al_2O_3.

D. Further notes

The diffusion in alumina, especially in experimental samples with doping impurities, is a very complex process probably involving many mechanisms and aspects (as reviewed elegantly in Ref. 21). In this paper, we only studied the diffusion processes of O and Al atoms via vacancy-atom exchange mechanism in bulk alumina as well as several modeled grain boundaries. Therefore, our work should be regarded as a starting point to theoretically investigate the diffusion in alumina using the first-principles transition state calculations. Below, we discuss how these type of theoretical calculations could be used to address the issues related to the actual diffusion processes in alumina.

(1) It was noticed in experimental measurements that some non-Fickian "tails", which appeared in the O and Al diffusion profiles of unannealed alumina specimens, could be removed through annealing the specimens at high temperature.[8,46] This phenomenon indicates that some material processes must occur in the alumina samples during annealing so that some fast routes (or mechanisms) for diffusion existing in the unannealed samples are eliminated. However, little is known regarding the nature of the observed non-Fickian behavior and the subsequent material processes of annealing. It was proposed that the non-Fickian behavior of alumina might be related to the atomic diffusion via dislocation networks or subgrain boundaries.[10,47] This explanation is not well consistent with the finding that the magnitude of the non-Fickian "tails" was insensitive to the dislocation densities in the samples.[46] Thus, Heuer proposed in Ref. 21 that the non-Fickian behavior of alumina could be a result of nonequilibrium point defect population. In this aspect, first-principles calculations can be employed to evaluate the energetics of diffusion along dislocations and the diffusion of Frenkel pairs (a vacancy plus an interstitial). In this paper, we have reported the energies of some transition states for a migrating atom between two vacancies in alumina.

(2) Conventional defect diffusion mechanism suggests that the diffusivity of materials be strongly dependent on the concentration of the defects in the material samples. However, it was found that the diffusivity of oxygen in alumina was not quite sensitive to the amount of point defects as expected.[3,21,48] Neither varying the partial pressure of O_2 gas[49] nor doping alumina with aliovalent solutes[48] would induce significant changes to the oxygen diffusivity in α-Al_2O_3 specimens. To explain these experimental data, many diffusion mechanisms, such as vacancy-atom exchange mechanism,[3] interstitial mechanism,[21,50] point defect cluster mechanism,[49] AlO divacancy mechanism,[4] and hydroxyl/peroxide mechanism,[21] have been proposed in the literature. In this paper, we assumed that the lattice diffusion of O in alumina was accomplished via vacancy-atom exchange mechanism. Evidently, some further first-principles studies are desired to extensively examine all these other possible diffusion mechanisms and to predict which mechanism is most favorable in α-Al_2O_3.

(3) Most often, the experimental samples of alumina contain various impurities.[3,8,9] Some impurities such as Si,[51] Mg,[51] Ca,[52] and Y[13] prefer segregating themself onto the grain boundaries from the bulk alumina. As a result, even if the concentrations of the impurities are low in the whole sample, the GB regions of the sample could have quite high concentration of the impurities.[51] Moreover, the segregation of impurities could even alter the geometric structures of the GBs.[53] Consequently, the path and activation energy for the diffusion on the GBs having segregated impurities might deviate appreciably from what we calculated here for pure α-Al_2O_3. Complementary to experimental measurements, the first-principles transition state calculations can help to quantify the effect of the grain boundary segregation on the diffusion processes in alumina.

VI. CONCLUSIONS

In this paper, we employed first-principles DFT method to predict the activation energies for O and Al diffusion via vacancy-atom exchange mechanism in the bulk lattice, high-energy $\Sigma3(0001)$ GBs, and low-energy $\Sigma3(10\bar{1}0)$ GBs of α-Al_2O_3. We found that each O atom had four nearest-neighboring Al atoms, whereas each Al atom had six nearest-neighboring O atoms in the bulk crystal. In the interphase of high-energy $\Sigma3(0001)$ GBs, the O atoms were still fourfold coordinated, and the Al atoms were still sixfold coordinated. However, the arrangement of the neighboring atoms around the O and Al atoms differs much in the $\Sigma3(0001)$ GBs and in the bulk crystal in terms of the angles of adjacent Al-O bonds. The O atoms could be threefold coordinated, fourfold coordinated, or fivefold coordinated, while all the Al atoms are sixfold coordinated in the interphase of low-energy $\Sigma3(10\bar{1}0)$ GBs. Moreover, it was found that the formation energies of O or Al vacancies were lower in the GBs than in the bulk crystal. In particular, the O vacancy formation energy could be lower by 1.30 eV in the O-terminated $\Sigma3(0001)$ GB and by 0.38 eV in the $\Sigma3(10\bar{1}0)$ GBs than the value of bulk crystal. More pronouncedly, the Al vacancy formation energy could be lower by 3.39 eV in the Al-terminated $\Sigma3(0001)$ GB and by 0.95 eV in the glide-mirror $\Sigma3(10\bar{1}0)$ GB than that in bulk crystal. Hence, our DFT calculations revealed that the vacancy formation energy would be reduced in the grain boundaries as compared to in bulk crystal of α-Al_2O_3.

Furthermore, we investigated the O and Al elementary diffusive jumps at an atomistic level and predicted the activation energies for these lattice and grain boundary diffusions in alumina. In bulk α-Al_2O_3, we identified four elementary jumps for O lattice diffusion in Fig. 5 and four elementary jumps for Al lattice diffusion in Fig. 6. These elementary diffusive jumps can be used to construct any long-range diffusion routes in the bulk lattice. It was predicted in Table III that the activation energy for O lattice diffusion varied from 3.58 to 5.03 eV, while the activation energy for Al lattice diffusion ranged from 1.80 to 3.17 eV. In comparison, the activation energy for O lattice diffusion was measured to be 5.50 eV (Ref. 12) to 8.15 eV (Ref. 7), while the activation energy for Al lattice diffusion was 5.29 eV (Ref. 8) in single-crystal alumina. Thus, it appears that our calculations underestimate the activation energy of lattice diffusion in alumina. Comparing the activation energies of O and Al elementary jumps, we inferred that Al lattice diffusion required less energy and should be faster than O lattice

diffusion. This finding is consistent with the experimental observation that the Al lattice diffusion was faster than the O lattice diffusion in α-Al_2O_3.[6,8]

In the interphase of high-energy $\Sigma3(0001)$ GBs, the diffusion of O and Al atoms is restricted within the (0001) plane. The activation energies of O diffusion in the O-terminated $\Sigma3(0001)$ GB were predicted to be 1.26 and 1.29 eV. In comparison, the activation energies of O lattice diffusion in the (0001) plane of α-Al_2O_3 were 3.58 and 5.03 eV. In the case of Al diffusion, the activation energies were calculated to be 0.64 and 1.22 eV in the Al-terminated $\Sigma3(0001)$ GB, while it was found to be 1.80 eV in the bulk crystal. Consequently, our DFT results indicated that the diffusion activation energy would be lower in the high-energy GBs than the bulk alumina. In the interphase of low-energy $\Sigma3(10\bar{1}0)$ GBs, the diffusion of O and Al atoms are restricted along the [0001] direction. We found that the activation energy for O grain boundary diffusion could be 4.13 eV, and the activation energy for Al grain boundary diffusion could be 3.22 eV in the screw-rotation $\Sigma3(10\bar{1}0)$ GB. In contrast, the calculated activation energy for the corresponding O and Al lattice diffusions was 4.11 and 3.17 eV, respectively. Hence, our DFT results revealed that the diffusion activation energy could be even higher in the low-energy GBs than the bulk crystal. This finding from our theoretical calculations supports previous experimental results[8,13,15] that the activation energy of atom diffusion in polycrystal alumina could be even higher than that in single-crystal alumina.

Therefore, we have attained atomistic details and energetics about the lattice and grain boundary diffusion processes in alumina using DFT calculation method. This knowledge will help us to further understand the formation mechanism and predict the growth rate of α-Al_2O_3 scales, which are able to protect the Al-containing materials at high temperature and under harsh operating environments.

ACKNOWLEDGMENTS

G.F. Wang would like to acknowledge the research grants from the Chemical Sciences Research Programs, Office of Basic Energy Sciences, US Department of Energy (Grant No. DE-FG02-09ER16093).

*Corresponding author: guw8@pitt.edu

[1] R. Prescott and M. J. Graham, Oxid. Met. **38**, 233 (1992).
[2] A. H. Heuer, D. B. Hovis, J. L. Smialek, and B. Gleeson, J. Am. Ceram. Soc. **94**, S146 (2011).
[3] J. H. Harding, K. J. W. Atkinson, and R. W. Grimes, J. Am. Ceram. Soc. **86**, 554 (2003).
[4] R. H. Doremus, J. Appl. Phys. **100**, 101301 (2006).
[5] Y. Oishi and W. D. Kingery, J. Chem. Phys. **33**, 480 (1960).
[6] A. E. Paladino and W. D. Kingery, J. Chem. Phys. **37**, 957 (1962).
[7] D. J. Reed and B. J. Wuensch, J. Am. Ceram. Soc. **63**, 88 (1980).
[8] M. Le Gall, B. Lesage, and J. Bernardini, Philos. Mag. A **70**, 761 (1994).
[9] D. Clemens, K. Bongartz, W. J. Quadakkers, H. Nickel, H. Holzbrecher, and J. S. Becker, Fresenius J. Anal. Chem. **353**, 267 (1995).
[10] D. Prot and C. Monty, Philos. Mag. A **73**, 899 (1996).
[11] A. H. Heuer and K. P. D. Lagerlöf, Philos. Mag. Lett. **79**, 619 (1999).
[12] T. Nakagawa, A. Nakamura, I. Sakaguchi, N. Shibata, K. P. D. Lagerlöf, T. Yamamoto, H. Haneda, and Y. Ikuhara, J. Ceram. Soc. Jpn. **114**, 1013 (2006).
[13] T. Nakagawa, I. Sakaguchi, N. Shibata, K. Matsunaga, T. Mizoguchi, T. Yamamoto, H. Haneda, and Y. Ikuhara, Acta Mater. **55**, 6627 (2007).
[14] P. Fielitz, G. Borchardt, S. Ganschow, R. Bertram, and A. Markwitz, Solid State Ionics **179**, 373 (2008).
[15] T. Nakagawa, H. Nishimura, I. Sakaguchi, N. Shibata, K. Matsunaga, T. Yamamoto, and Y. Ikuhara, Scr. Mater. **65**, 544 (2011).
[16] P. W. M. Jacobs and E. A. Kotomin, J. Am. Ceram. Soc. **77**, 2505 (1994).
[17] J. H. Harding and D. J. Harris, Phys. Rev. B **63**, 094102 (2001).
[18] J. Carrasco, N. Lopez, and F. Illas, Phys. Rev. Lett. **93**, 225502 (2004).
[19] U. Aschauer, P. Bowen, and S. C. Parker, Acta Mater. **57**, 4765 (2009).
[20] I. Milas, B. Hinnemann, and E. A. Carter, J. Mater. Chem. **21**, 1447 (2011).
[21] A. H. Heuer, J. Euro. Ceram. Soc. **28**, 1495 (2008).
[22] E. Wimmer, R. Najafabadi, G. A. Young, Jr., J. D. Ballard, T. M. Angeliu, J. Vollmer, J. J. Chambers, H. Niimi, J. B. Shaw, C. Freeman, M. Christensen, W. Wolf, and P. Saxe, J. Phys.: Condens. Matter **22**, 384215 (2010).
[23] G. Kresse and J. Hafner, Phys. Rev. B **47**, 558 (1993).
[24] G. Kresse and J. Furthmüller, Comput. Mater. Sci. **6**, 15 (1996).
[25] G. Kresse and D. Joubert, Phys. Rev. B **59**, 1758 (1999).
[26] J. P. Perdew, K. Burke, and M. Ernzerhof, Phys. Rev. Lett. **77**, 3865 (1996).
[27] G. Henkelman, B. P. Uberuaga, and H. Jónsson, J. Chem. Phys. **113**, 9901 (2000).
[28] H. J. Monkhorst and J. D. Pack, Phys. Rev. B **13**, 5188 (1976).
[29] See Supplemental Material at http://link.aps.org/supplemental/10.1103/PhysRevB.87.214105 for accuracy validation of our GB simulation method.
[30] S. Zhang, O. Y. Kontsevoi, A. J. Freeman, and G. B. Olson, Phys. Rev. B **85**, 214109 (2012).
[31] W. Setyawan and R. J. Kurtz, Scr. Mater. **66**, 558 (2012).
[32] H. Zhou, Y. Liu, C. Duan, S. Jin, Y. Zhang, F. Gao, X. Shu, and G. Lu, J. Appl. Phys. **109**, 113512 (2011).
[33] K. Nakamura, T. Mizoguchi, N. Shibata, K. Matsunaga, T. Yamamoto, and Y. Ikuhara, Phys. Rev. B **75**, 184109 (2007).
[34] A. G. Marinopoulos, S. Nufer, and C. Elsässer, Phys. Rev. B **63**, 165112 (2001).
[35] J. C. Boettger, Phys. Rev. B **55**, 750 (1997).
[36] H. d'Amour, D. Schiferl, W. Denner, H. Schulz, and W. B. Holzapfel, J. Appl. Phys. **49**, 4411 (1978).
[37] T. Geipel, J. B. Bilde-Sorensen, B. F. Lawlor, P. Pirouz, K. P. D. Lagerlof, and A. H. Heuer, Acta Mater. **44**, 2165 (1996).

[38]S. Fabris, S. Nufer, C. Elsässer, and T. Gemming, Phys. Rev. B **66**, 155415 (2002).
[39]I. Tanaka, K. Tatsumi, M. Nakano, and H. Adachi, J. Am. Ceram. Soc. **85**, 68 (2002).
[40]K. Matsunaga, T. Tanaka, T. Yamamoto, and Y. Ikuhara, Phys. Rev. B **68**, 085110 (2003).
[41]J. Carrasco, J. R. B. Gomes, and F. Illas, Phys. Rev. B **69**, 064116 (2004).
[42]N. D. M. Hine, K. Frensch, W. M. C. Foulkes, and M. W. Finnis, Phys. Rev. B **79**, 024112 (2009).
[43]A. Brokman, P. D. Bristow, and R. W. Balluffi, J. Appl. Phys. **52**, 6116 (1981).
[44]M. R. Sorensen, Y. Mishin, and A. F. Voter, Phys. Rev. B **62**, 3658 (2000).
[45]D. Farkas, J. Phys.: Condens. Matter **12**, R497 (2000).
[46]K. P. R. Reddy and A. R. Cooper, J. Am. Ceram. Soc. **65**, 634 (1982).
[47]M. Le Gall, A. M. Huntz, B. Lesage, and C. Monty, Philos. Mag. **73**, 919 (1996).
[48]K. P. D. Lagerlof, T. E. Mitchell, and A. H. Heuer, J. Am. Ceram. Soc. **72**, 2159 (1989).
[49]J. D. Cawley, J. W. Halloran, and A. R. Cooper, J. Am. Ceram. Soc. **74**, 2086 (1991).
[50]D. S. Phillips, T. E. Mitchell, and A. H. Heuer, Philos. Mag. **42**, 417 (1980).
[51]K. L. Gavrilov, S. J. Bennison, K. R. Mikeska, and R. Levi-Setti, Acta Mater. **47**, 4031 (1999).
[52]R. F. Cook and A. G. Schrott, J. Am. Ceram. Soc. **71**, 50 (1988).
[53]S. Lartigue-Korinek, D. Bouchet, A. Bleloch, and C. Colliex, Acta Mater. **59**, 3519 (2011).